Rock and Soil Mechanics

Volume 41 | Issue 2 Article 13

9-27-2020

Experimental study and engineering application of coupling performance between distributed embedded optical fiber and tunnel lining

Gong-yu HOU
School of Mining Engineering, Xinjiang Institute of Engineering, Urumqi, Xinjiang 830091, China

Bing-bing XIE
Guodian United Power Technology Co., Ltd, Beijing 100039, China

Yu-chen HAN
School of Mechanics and Civil Engineering, China University of Mining and Technology(Beijing), Beijing 100083, China

Tao HU
School of Mechanics and Civil Engineering, China University of Mining and Technology(Beijing), Beijing 100083, China

See next page for additional authors

Custom Citation

HOU Gong-yu, XIE Bing-bing, HAN Yu-chen, HU Tao, LI Zi-xiang, YANG Xing-kun, ZHOU Tian-ci, XIAO Hai-lin, . Experimental study and engineering application of coupling performance between distributed embedded optical fiber and tunnel lining[J]. Rock and Soil Mechanics, 2020, 41(2): 714-726.

Experimental study and engineering application of coupling performance between distributed embedded optical fiber and tunnel lining

Authors

Gong-yu HOU, Bing-bing XIE, Yu-chen HAN, Tao HU, Zi-xiang LI, Xing-kun YANG, Tian-ci ZHOU, and Hai-lin XIAO

Rock and Soil Mechanics 2020 41(2): 714–726 ISSN 1000–7598
https: //doi.org/10.16285/j.rsm.2019.5371 rocksoilmech.researchcommons.org/journal

Experimental study and engineering application of coupling performance between distributed embedded optical fiber and tunnel lining

HOU Gong-yu[1, 2], XIE Bing-bing[1,3], HAN Yu-chen[1], HU Tao[1], LI Zi-xiang[1], YANG Xing-kun[4], ZHOU Tian-ci[1], XIAO Hai-lin[1]

1. School of Mechanics and Civil Engineering, China University of Mining and Technology(Beijing), Beijing 100083, China
2. School of Mining Engineering, Xinjiang Institute of Engineering, Urumqi, Xinjiang 830091, China
3. Guodian United Power Technology Co., Ltd, Beijing 100039, China
4. China Railway Eighteen Bureaus Group Rail Transportation Engineering Co., Ltd., Tianjin 300350, China

Abstract: The coupling performance of embedded optical fiber and tunnel lining is studied using theoretical and experimental methods, and then is verified in practical engineering. We calculate the strain transmission efficiency of fiber by modeling and analyzing the structure of optical fiber, intermediate and matrix. Totally two sets of experiments are designed. The reinforced concrete beams with 6 kinds of optical fiber layout are designed in same working condition. The multistage loading was carried out at a single point in the way of displacement control. At the same time, 6 optical fibers are monitored based on the BOFDA (Brillouin optical frequency domain analysis) technology. The results of two different groups show the similar law: six optical fibers can effectively monitor the process of beam loading from the stage of beginning to the stage of yielding, and the coupling between fiber and beam is good in this process. When the reinforcement begins to yield to the failure process, the fiber strain no longer increases, even decreases or presents the state of fiber fracture, and the coupling of the fiber and the beam is poor in this process. Except for the slotted embedded fiber, the effective monitoring strain difference is 3 000×10^{-6}, the effective strain difference of the remaining fiber is 2 000×10^{-6}. Under the condition of long distance (>>146 mm) embedding, the strain transmission efficiency of optical fiber is close to 100%. Taking the underground excavation section of the new built airport in Beijing as an example, the fiber is embedded in the two waist and vault of the initial lining, and the construction process of the CRD method is monitored by monitoring fiber. Monitoring results show that the embedding technology is feasible, which is able to provide references and valued suggestions for other related monitoring projects.

Keywords: distributed burying; tunnel lining; coupling performance; BOFDA technology

1 Introduction

In recent years, fiber optic sensing (network) monitoring technologies such as BOTDR (Brillouin Optical Time Domain Reflectometer strain/temperature measurement technology), BOTDA (Brillouin Optical Time Domain Analysis strain/ temperature measurement technology), ROTDR (Raman Optical Time Domain Reflectometry strain/temperature measurement technology) , the FBG (Fiber Bragg Grating measurement technology) , etc. [1–3], have been used in ground and geological engineering [4–5], mine safety monitoring [6], pipeline monitoring [7], the distributed optical fiber sensing technology has developed rapidly. Wherein, in the monitoring of underground engineering fibers embedded test structures usually requires, the construction should be considered in the following aspects: (i) ensure the safety of the optical fiber, the survival rate; (ii) minimize optical losses of the optical fiber; (iii)enhance the coupling between the optical fiber and the structure to be tested so as to the monitoring data reflects the real deformation;(iv)minimize disturbance to the original structure; (v) economy of optical fiber installation; (vi) installation process should be simple and convenient. At present, most of the optical fiber layout methods in monitoring projects rely on empirical methods, which do not give strong guidance to actual projects. Therefore, it is very necessary to carry out a systematic study on the layout of the optical fiber, so as to give a stronger guidance to the actual monitoring project.

At present, some scholars have applied fiber optic sensing technology to the safety monitoring of concrete structures. Ye et al.[8] respectively arranged distributed optical fiber sensors on the longitudinal surface of the beam and the outer surface of the concrete beam to determine the cracking load and crack distribution of the concrete beam. Bao et al. [9] developed an optical fiber sensor based on optical time domain reflection to detect concrete crack. Hou et al.[10–11] studied the sheath effect and zigzag layout technology of optical fiber, solved the

Received: 18 February 2019 Revised: 12 May 2019
This work was supported by the Central University Major Achievement Transformation Project in Beijing (ZDZH20141141301) and the National Natural Science Fund Committee and Shenhua Group Co., LTD. Jointly Funded Key Projects (U1261212).
First author: HOU Gong-yu, male, born in 1965, PhD, Professor, Doctoral supervisor, Research interest: rock mechanics and rock engineering. E-mail: hgyht@126.com
Corresponding author: XIE Bing-bing, male, born in 1991, PhD candidate, specializing in rock mechanics and tunnel health monitoring. E-mail: XIE817824@163.com

problem of optical fiber selection and indirectly improved the sensitivity of optical fiber strain gauge by changing the layout of optical fiber. Liu [12] proposed to monitor the corrosion of steel bars from the stress-strain changes of steel bars and surrounding concrete caused by corrosion. By analyzing the relationship between the strain changes and the corrosion of steel bars, the principle and method of monitoring the corrosion of steel bars were given. Chen et al.[13] applied the distributed optical fiber sensing technology to the horizontal load test of single pile, which can be extended to the quality inspection and long-term safety monitoring of pile foundation. Li et al. [14] adopted the BOFDA to test the internal force of the pile body of bored pile by rotary excavation while the vertical static load test on the bored pile was performed, so as to provide technical basis and suggestions for optimizing the design of the pile and guiding the construction of the pile.These researches have made useful explorations for the application of optical fiber sensing technology in civil engineering.

How to realize the application of BOFDA technology, the focus is the monitoring mechanism, and the key technology is the method of laying out the sensing fiber on the object to be measured. Based on BOFDA monitoring technology, this paper makes further research on the way of laying optical fibers on concrete structures, focusing on the coupling performance of six different laying modes of optical fibers and reinforced concrete beams, and makes a comparative analysis with strain gauges. The fiber layout method with the best coupling performance is given, and it is further verified in actual engineering.

2 Theoretical analysis of fiber strain transfer mechanism

The main component of the bare fiber of the optical fiber sensor is silicon dioxide, which is a brittle material and its shear resistance is poor and it is easy to break. Civil engineering construction is a typical extensive operation, so in practical applications, no matter what kind of layout the optical fiber adopts, it is necessary to glue the bare optical fiber part or retain the coating to protect it. Because the physical properties of the adhesive layer or the coating layer are different from those of the bare fiber, the structural strain is inconsistent with the strain measured by the optical fiber sensor. It is necessary to establish a model to simulate the optical fiber embedded in the concrete structure, and analyze and calculate the optical fiber strain transfer rate. Because the optical fiber sensor uses a distributed embedded layout craft, the sensor and structure can be simplified into three concentric cylinders: the bare fiber part is a central cylinder, the adhesive layer or packaging layer is an intermediate structure, and the structure to be tested is a base structure.

2.1 Assumption

(1)The materials are all linear elastic, and the base structure is subjected to uniform strain along the direction of the optical fiber, and then the optical fiber is strained by the bonding length.

(2)The mechanical properties of the fiber core and cladding are the same.

(3)The interfaces between the optical fiber and the intermediate structure, and the intermediate structure and the substrate are tightly combined, without falling off.

The optical fiber, intermediate structure and base structure are connected to each other and the stress of each part, as shown in Fig.1.

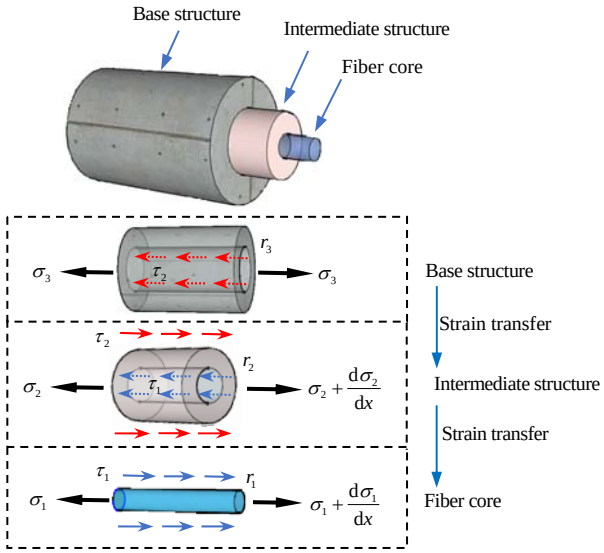

Fig.1 Mechanical models of optical fibers, intermediates and matrix structures

among them, σ_1 is the axial stress on the fiber core, r_1 is the radius of the fiber core, E_1 is the elastic modulus of the fiber core, ε_1 is the strain of fiber core; τ_1 is the strain transfer force between the fiber core and the intermediate structure; σ_2 is axial stress on the intermediate structure, E_2 is the elastic1 modulus of the intermediate structure, ε_2 is the strain of the fiber core; r_2 is the radius from the center of the optical fiber core to the outer boundary of the cross section of intermediate structure; τ_2 is the strain transfer force between the intermediate and the matrix structures; σ_3 is the axial stress on the base structure, ε_3 is the strain of the base structure, r_3 is the radius from the center of the fiber core to the outer edge of the intermediate structure on the base structure, which can be generally regarded as infinity.

2.2 Theoretical analysis

An analysis of a short section of the fiber can be obtained

$$\frac{\mathrm{d}\sigma_1}{\mathrm{d}x}=-\frac{2\tau(x,r_1)}{r_1} \tag{1}$$

Take a section of the intermediate structure and analyze it to get

$$\tau(x,r)=\frac{r_1}{r}\tau_1(x,r_1)-\frac{r^2-r_1^2}{2r}\frac{\mathrm{d}\sigma_2}{\mathrm{d}x} \tag{2}$$

Substituting Eq. (1) into Eq. (2) gives

$$\tau(x,r)=-\frac{r_1^2}{2r}\frac{\mathrm{d}\sigma_1}{\mathrm{d}x}-\frac{r^2-r_1^2}{2r}\frac{\mathrm{d}\sigma_2}{\mathrm{d}x} \tag{3}$$

Because the radial deformation of the fiber is very small, the Poisson effect can be ignored.

$$\begin{aligned}\tau(x,r)=&-\frac{r_1^2}{2r}E_1\frac{\mathrm{d}\varepsilon_1}{\mathrm{d}x}-\frac{r^2-r_1^2}{2r}E_2\frac{\mathrm{d}\varepsilon_2}{\mathrm{d}x}=\\&-\frac{E_1r_1^2}{2r}\left(\frac{\mathrm{d}\varepsilon_1}{\mathrm{d}x}+\frac{r^2-r_1^2}{2r}\frac{E_2}{E_1}\frac{\mathrm{d}\varepsilon_2}{\mathrm{d}x}\right)\end{aligned} \tag{4}$$

Due to simultaneous deformation of the optical fiber and the intermediate layer, their strain rates are similar, that is

$$\frac{\mathrm{d}\varepsilon_1}{\mathrm{d}x}\cong\frac{\mathrm{d}\varepsilon_2}{\mathrm{d}x} \tag{5}$$

Because the difference between the elastic modulus of the optical fiber and the intermediate layer is large (usually more than 10 times), it can beconsidered that

$$\frac{r^2-r_1^2}{2r}\frac{E_2}{E_1}\frac{\mathrm{d}\varepsilon_2}{\mathrm{d}x}\cong o\left(\frac{\mathrm{d}\varepsilon_1}{\mathrm{d}x}\right) \tag{6}$$

$$\tau(x,r)=-\frac{r_1^2}{2r}\frac{\mathrm{d}\sigma_1}{\mathrm{d}x}=-\frac{r_1^2}{2r}E_1\frac{\mathrm{d}\varepsilon_1}{\mathrm{d}x} \tag{7}$$

Because the fiber is very thin and the aspect ratio is large, the radial displacement can be ignored, that is

$$\tau(x,r)=G_2\gamma(x,r)=G_2\left(\frac{\partial u}{\partial r}+\frac{\partial w}{\partial x}\right)\cong G_2\frac{\partial u}{\partial r} \tag{8}$$

where u is the axial displacement of the intermediate layer; $G_2=E_2/[2(1+u)]$ is the shear modulus of the intermediate layer; and $\gamma(x,r)$ is the shear strain.

Substituting Eq. (8) into Eq. (7) and integrating, we get

$$\int_{r_1}^{r_3}\left(G_2\frac{\partial u}{\partial r}\right)\mathrm{d}r=\int_{r_1}^{r_3}\left(-\frac{r_1^2}{2r}E_1\frac{\mathrm{d}\varepsilon_1}{\mathrm{d}x}\right)\mathrm{d}x \tag{9}$$

$$u_3-u_1=-\frac{E_1}{2G_2}\frac{\mathrm{d}\varepsilon_1}{\mathrm{d}x}r_1^2\ln\left(\frac{r_3}{r_1}\right)=-\frac{1}{k^2}\frac{\mathrm{d}\varepsilon_1}{\mathrm{d}x} \tag{10}$$

$$k^2=\frac{2G_2}{r_1^2E_1\ln\left(\frac{r_3}{r_1}\right)}=\frac{1}{(1+u)\frac{E_1}{E_2}r_1^2\ln\left(\frac{r_3}{r_1}\right)} \tag{11}$$

By deriving Eq. (10) from x, we can get

$$\frac{\mathrm{d}^2\varepsilon_1(x)}{\mathrm{d}x^2}-k^2\varepsilon_1(x)=-k^2\varepsilon_3 \tag{12}$$

Eq. (12) is the governing equation of the axial strain distribution of the optical fiber and its relationship with the substrate strain. Parameter k contains the effects of the elastic modulus and radius of the optical fiber and the intermediate layer. The general solution is

$$\varepsilon_1(x)=c_\mathrm{a}\mathrm{e}^{kx}+c_\mathrm{b}\mathrm{e}^{-kx}+\varepsilon_3 \tag{13}$$

where c_a and c_b are the integration constants determined by boundary conditions. Since the end where the optical fiber intersects with the middle layer is a free end face without strain transmission, the length of the optical fiber is set to $2L$ and the midpoint is the origin, so the boundary condition is

$$\varepsilon_1(L)=\varepsilon_1(-L)=0 \tag{14}$$

This boundary condition is equivalent to

$$\varepsilon_1(L)=0,\ \dot{\sigma}_1(0)=0\ \text{ or }\ \dot{\varepsilon}_1(0)=0 \tag{15}$$

That is, there is no shear stress at the midpoint of the fiber bonding part. Because of the symmetry, refer to Eq. (1). The boundary conditions determined by Eqs. (14) and (15) can get the same solution. Substituting the boundary conditions determined by Eq. (12) into Eq. (8), the integration constant is determined as

$$c_\mathrm{a}=c_\mathrm{b}=-\frac{\varepsilon_3}{2\cosh(kL)} \tag{16}$$

Therefore, the solution of Eq. (10), that is, the axial strain distribution in the fiber is

$$\varepsilon_1(x)=\varepsilon_3\left[1-\frac{\cosh(kx)}{\cosh(kL)}\right] \tag{17}$$

From this, the strain transfer rate of each point of the fiber bonding part [15] can be expressed as

$$a(x)=\frac{\varepsilon_1(x)}{\varepsilon_3}=1-\frac{\cosh(kx)}{\cosh(kL)} \tag{18}$$

In order to more directly represent the strain transfer rate of the fiber, taking the general physical parameters of the strained fiber core and intermediate layer in Table 1 as examples, and substituting them into Eq. (18), the strain transfer rates of each point of the embedded part of the fiber are shown in Fig. 2

It can be seen in Fig. 2 that the strain transfer rate at both ends of the optical fiber is the smallest, and the middle transmission rate is close to 100%, and the overall shape is "convex". Theoretically, there exists a length of $2L$ that makes the strain transmission rate of at least 90% of the fiber length is greater than or equal to 95%, that is,

$$\alpha(0.9L) \geqslant 95\% \tag{19}$$

which is

$$\alpha(0.9L) = 1 - \frac{\cosh(k \times 0.9L)}{\cosh(kL)} \geqslant 0.95 \tag{20}$$

Table 1 Physical properties of optical fibers and intermediates

Fiber flexibility modulus E_1 / Pa	Middle layer elastic modulus E_2 / Pa	Middle layer Poisson's ratio μ	Middle layer outer diameter r_3 / μm	Optical fiber outer diameter r_1 / μm	Optical fiber length L / mm
7.2×10^{10}	3×10^{9}	0.3	600	62.5	40

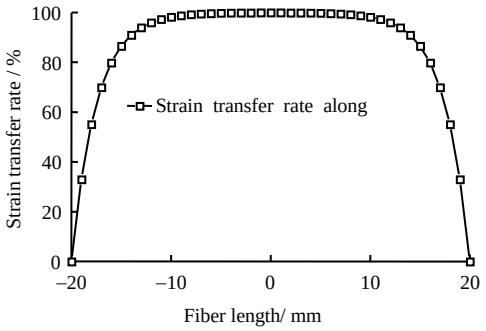

Fig.2 Fiber strain transfer rate of 40 mm in length

$$L \geqslant 30/k \approx 73 \text{ mm},\ 2L \geqslant 146 \text{ mm} \tag{21}$$

From Eqs.(20) and (21), we can obtain when the embedding length of the optical fiber is longer than 146 mm, the strain transfer rate can be 95% in at least 90% of the length range in the middle of the optical fiber, and the longer the embedding length, the higher the efficiency of the strain transfer, which can be used as a general rule. Generally, in distributed optical fiber sensing projects, if the embedded length of optical fibers is much longer than 146 mm, the difference caused by the types of strain optical fibers can be ignored, it can be thought that the strain transfer efficiency is close to 100%.

The above theory has assumptions. There are many factors that affect the strain transmission of optical fibers in actual engineering. Therefore, further experiments and engineering are needed to explore the coupling effect between embedded optical fibers and base structure.

3 Laying of optical fiber in reinforced concrete lining

3.1 Manufacture of reinforced concrete beam specimens

A tunnel concrete lining incorporates beams, plates (shells), columns and other structures. But in order to better test the strain change of optical fiber in the reinforced concrete lining, the reinforced concrete beam components are designed in this study. The size of reinforced concrete model beam is: 1 900 mm × 120 mm × 200 mm (length × width × height), the concrete strength grade is C30, the secondary reinforcement HRB335 with diameter of 16 mm is selected for the lower stressed reinforcement, the stirrup with diameter of 8 mm, the erection reinforcement with diameter of 10 mm and the thickness of protective layer with thickness of 22 mm. In order to eliminate accidental factors and accidents, a total of two groups of model beams were made.

3.2 Optical fiber and strain gauge layout

Optical fiber and its fragile nature are in sharp contrast with the extensive concrete construction. How to ensure the survival rate of the fragile fiber in the concrete construction process is a key problem to be solved in the application of sensing fiber in practical engineering

At present, in practical engineering, there are two main layouts of optical fiber, i.e. surface-mounted and embedded. The six layouts in this paper are derived from this. Mode 1(Fiber 1), the optical fiber is directly tied to the bottom stressed steel bar with nylon ribbon , and the ribbon spacing is 200 mm; Mode 2(Fiber 2), a ditch with a width of 3 mm, a depth of 3 mm) is grooved along the length of the steel bar, then put the optical fiber into the groove and fill the groove with epoxy resin to bond and protect the optical fiber; Mode 3(Fiber 3), the optical fiber is wrapped around the steel bar to simulate the misalignment of the optical fiber during installation; Mode 4(Fiber 4), the optical fiber is arranged in the same position as the optical fiber 1, and the number of nylon ribbon is doubled and the spacing is adjusted to 100 mm; Mode 5(Fiber 5), after curing of the reinforced concrete beam, at the same height of the bottom stressed reinforcement, the optical fiber shall be embedded and sealed with cement mortar after slotting (width×depth is 10 mm×10 mm) on the beam surface along the beam length direction; Mode 6(Fiber 6), at the same height on the other side of position of Fiber 5, use epoxy resin to paste the optical fiber on the surface of reinforced concrete beam.

For comparative verification, strain gauges were placed in reinforced concrete beams. Grind the bottom stressed steel bar flat. In order to avoid short-circuit, paste the strain gauge on the steel bar after applying insulating paper on the steel bar, and then coat the strain gauge with epoxy resin to protect the strain. Strain gauges ② and ⑤ are respectively arranged in the middle of the bottom rebar, while the remaining 4 strain gauges are installed at the side locations of 200 mm from the strain gauges ② and ⑤. As shown in Fig. 3.

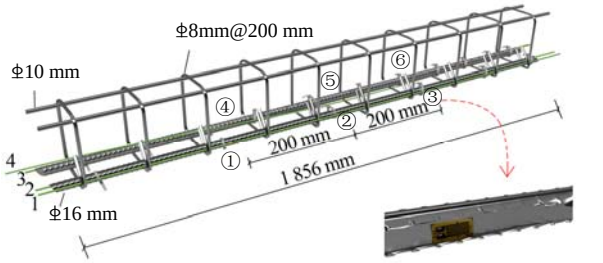

Polish the surface of steel bar and then paste strain gauge

(a) Reinforcement cage size and position of strain gauge

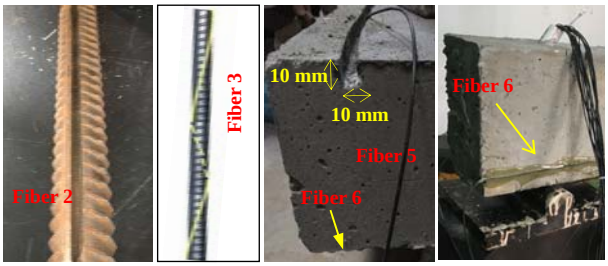

(b) Embedded locations of optical fibers inside and outside steel bar and concrete beams

Fig.3 Layout of optical fiber and strain gauge in reinforced concrete beams

4 BOFDA monitoring technology and loading test system

4.1 BOFDA distributed optical fiber monitoring technology

This test uses a German-made fTB2505 Brillouin optical frequency domain fiber strain / temperature analyzer based on BOFDA technology. In this test, the test parameters of the instrument are set as follows: pulse width is 10 ns, strain test accuracy is $\pm 2 \times 10^{-6}$, refractive index is 1.468, and the starting and ending frequency of the instrument are 10.5 to 11.0 GHz. This range can theoretically measure 12 500×10^{-6} large strain without overflowing the Brillouin frequency, the center frequency of the fiber $f_B(0) = 10.839$ GHz, and the frequency interval is 5 MHz. In order to make the data more accurate, the minimum sampling interval of the instrument is 0.05 m and the spatial resolution is 0.2 m.

4.2 Test strain fiber type

The new strained optical fiber with a diameter of 2 mm and a sheath material of polyurethane is a strained optical fiber specially developed to monitor strain on the basis of ordinary strained optical fiber. It not only has good ductility, but also solves the problem of relative slippage between the traditional sheathed fiber and sheath, which is suitable for cyclic load, as shown in Fig.4.

4.3 Loading test method

The test uses a microcomputer-controlled electro- hydraulic servo multi-point coordinated loading fatigue test system with a maximum uniaxial loading limit of 500 kN. The test uses displacement loading control. The overall layout of the laboratory is shown in Fig. 5 (a).

The beam is loaded by simply supported beam, as shown in Fig. 5(b). 5 kN is first loaded for preloading. After the load is stabilized for 5 minutes , the initial data of 6 strain gauges and 6 fibers are measured. The test is divided into two groups: the loading rate of the first group of beams is 2 mm/100 s, after the initial data is measured, the load is exerted according to this loading rate. After the loading is completed, strain gauges and optical fiber strain measurements are performed. fTB2505 requires six optical fibers to be measured separately, with a loading duration of about 15 minutes, then the next stage is loaded; the loading rate of the second group of beams is 3 mm/100 s, the remaining steps are the same as the first group.

By using this loading method, the coupling relationship between distributed optical fiber sensors and reinforced concrete structures can be preliminarily investigated, it can provide references and suggestions for the way of laying optical fibers in tunnel linings.

Fig.4 New type of tight sheathed strain sensing fiber

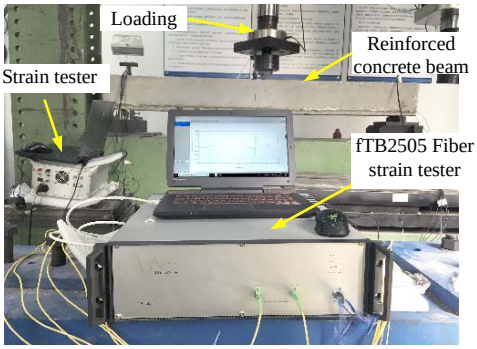

(a) Laboratory layout

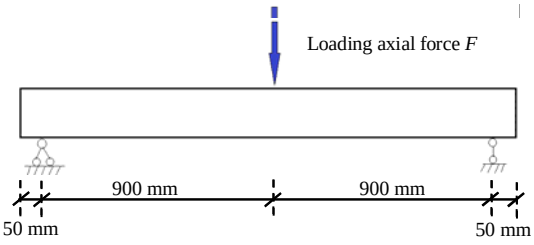

(b) Beam loading diagram

Fig.5 Laboratory layout and loading sketch

5 Test results and analysis

5.1 Reinforced concrete beam loading path

According to the loading method in Section 4.3 and measured loading data, the loading path of the reinforced concrete beam is shown in Fig.6. Its abscissa is the vertical loading displacement of the loading equipment in the middle of the beam, and the ordinate is the loading axial force corresponding to each loading displacement.

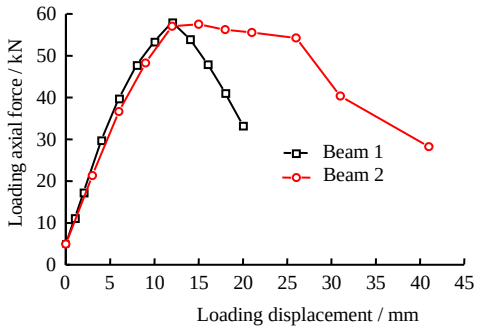

Fig.6 Loading path diagram of reinforced concrete beam

5.2 Yield strain analysis of steel bars

The grade of the reinforced steel used in this test is HRB335, its yield strength is 335 MPa, and its elastic modulus is 210 GPa. Therefore, its yield strain is

$$\varepsilon_{\text{yield}}=\frac{\sigma_{\text{yield}}}{E}=\frac{335\ \text{MPa}}{210\ 000\ \text{MPa}}\approx 0.16\%=1\ 600\times10^{-6} \tag{22}$$

According to Eq.(22), when the strain of HRB335 steel bar reaches $1\ 600\times10^{-6}$, the steel bar begins to enter the yield stage.The ultimate tensile strain of longitudinal tensioned reinforcement in a bending member is 0.01[16], so the ultimate tensile strain of reinforcement is $10\ 000\times10^{-6}$. Fiber optic has a tensile limit of $15\ 000\times10^{-6}$ and can theoretically monitor the entire process of steel bar from elastic deformation to initial yield until reaching the ultimate tensile strain.

5.3 Analysis of strain gauge strain in beam

According to the loading path, the data of six strain gauges are shown in Fig.7. The theoretical value of strain gauge is calculated based on elastoplastic mechanics and can be used as a reference value. Analysis of the measured values of the strain gauges shows:

Except for the measured values of No.1 and No.4 strain gauges in beam 1, which differ greatly from the theoretical values, the measured values of other strain gauges are in good agreement with the theoretical values.

The measured value of strain gauge in beam 2 agrees well with the theoretical value before the peak load is reached; the peak load will be maintained for a period of time, i.e. the peak load range, at this time the steel bar begins to yield and at the same time the optical fiber strain starts to change abruptly. The difference between the measured values and the theoretical value of No.3 and No.6 strain gauges is large, so those values are not allowed to be used. The remaining strain values can be used as reference for measured values.

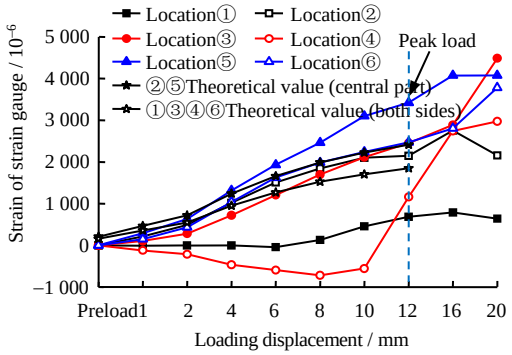

(a) Values of strain gauge in beam 1

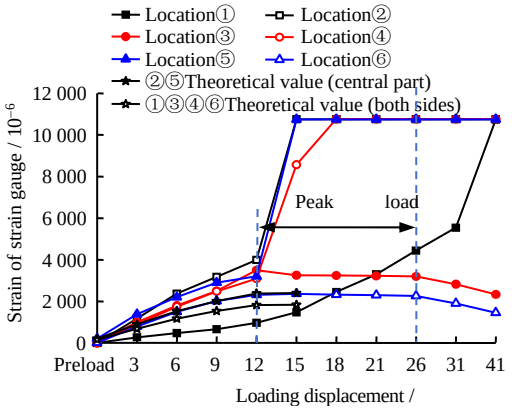

(b) Values of strain gauge in beam 2

Fig.7 Strain gauge data

The measured values of strain gauges No.1, No.4 in beam 1 and No.3 and No.6 in beam 2 differ greatly from the theoretical values. The possible reasons are installation errors. As two strain gauges are placed in the same position of reinforcement, the measured values of No.1 and No.4 in beam 1 can be deleted, referring to the measured values of No.6 and No.3 at the same position. Similarly, the measured values of No.3 and No.6 in beam 2 can be removed, referring to measuring values of No.4 and No.1.

5.4 Analysis of distributed optical fiber monitoring data in beams

Figures 8 and 9 are the fiber strain monitoring data of beam 1 and beam 2, respectively. In the figure, the abscissa represents the length distribution of the optical fiber, and the ordinate represents the strain value of each point along the length direction of the optical fiber.

A comprehensive analysis of the distributed optical fiber

monitoring data in beams 1 and 2 reveals that the 6 optical fibers as a whole have more obvious strain and deformation discrimination, but there are still differences between them. It is shown that both the optical fiber 1 (corresponding to Mode 1, 200 mm nylon ribbon spacing) and the optical fiber 4(corresponding to Mode 4, 100 mm nylon ribbon spacing) have large initial strain. The preliminary analysis shows that it is caused by concrete condensation and hardening, which does not affect the reading of the difference or the monitoring results. During the displacement loading process, the strain change of the optical fiber in the beam is basically consistent with the monitored value of the strain gauge.

The optical fiber 2(corresponding to Mode 2, buried inside the steel bar) has the best image effect. Before the peak load is reached, the measured strain value corresponds to the strain gauge strain value, but after the peak load, the strain value does not change or even decreases. According to the analysis, it is believed that the bonding effect of the epoxy resin bonding optical fiber to the reinforcement groove becomes poor after the peak load, resulting in poor strain transmission. This phenomenon is found in beams 1 and 2.

Because the optical fiber 3(corresponding to Mode 3) is twined on the steel bar, the optical fiber has a certain amount of margin. Therefore, the optical fiber does not have an excessively high initial strain during the concrete condensation and hardening process, and its strain value corresponds to the strain gauge before the peak load. After the peak load, the arrangement of optical fiber winding may cause the stress concentration in some positions to be too large and the strain mutation point will appear, leading to the monitoring distortion.

The optical fibers 5(corresponding to Mode 5) in beams 1 and 2 are slightly different. The strain changes in beam 1 before the peak load , and it is basically unchanged after the peak . The image effect of optical fiber in beam 2 is the best, and it can reflect the loading level before and after the peak.

The optical fiber 6(corresponding Mode 6) is a surface-adhesive arrangement type, which reflects the loading process at the low strain stage. After the peak load, the fiber strain will change abruptly, resulting in monitoring distortion.

As shown in Fig.10, the strain values of six optical fibers increase with the increase of loading displacement. The strain values of five optical fibers except No. 4 are basically the same as the strain values of strain gauges. The strain values of No.4 optical fibers are generally smaller than the measured value of strain gauge (about 300–500) $\times 10^{-6}$. However, the strain difference is consistent with those of the other five fibers; before the axis peak load is reached, the strain values of the six fibers increase orderly with the increase of load displacement, which conforms to the trend of strain change of reinforced concrete beams; but after the axis peak load, the strain values of the other five fibers do not increase much except that of No.3 fibers (wrapped around the steel bars) continue to increase. However, in practice, the strain and its growth rate of reinforced concrete beams increase after the axial peak load. At this time, the change trend of optical fiber strain value does not conform to the change trend of reinforced concrete beams.

To sum up, the layout of optical fiber has little influence on the monitoring results. All six optical fibers can effectively monitor the process from the beginning of loading to the beginning of yielding of reinforcement, in which the coupling between optical fiber and beam is the best. During the process from the beginning of yielding of reinforcement to the beam failure, the strain of optical fiber no longer increases or even decreases or presents the state of fiber fracture, in which the coupling between optical fiber and beam is poor. The effective monitoring strain difference (maximum strain value minus initial value) of embedded optical fiber (optical fiber No.5) is $3\ 000 \times 10^{-6}$, and that of optical fiber in other layouts is $2\ 000 \times 10^{-6}$.

6 Engineering applications

6.1 Project overview

The application case is at the second construction area of bid 07 of civil engineering of Beijing Rail Transit New Airport Line Phase I project. In this area, the construction of air shaft in the range of #2 interval to #1 interval is carried out. The construction mileage is from K33 + 208.249 to K35 + 545.227, including a concealed excavation section (90.995 m long), a shield shaft and open excavation section (130.9 m long) and a double line shield section (2119.7 m long).

In the concealed excavation section, the starting mileage is K35 + 454.232, the ending mileage is K35 + 545.227, the total length is 90.995 m, and the slope is 20 ‰. The section is a single-tunnel single-line horseshoe-shaped section with a structure covering 10.7 to 12 m. The excavation and initial support are constructed by the CRD method, and the secondary lining is made of a reinforced concrete structure. The width of the undercut tunnel is 8.9 m, the height is 9.09 m, the thickness of the initial lining structure is 300 mm, and the thickness of the protective layer is 30 mm. This monitoring project was mainly carried out in the right line project of the concealed excavated section .

6.2 Optical fiber layout

According to the actual construction conditions on site and the arrangement of optical fiber and the results in tests in Sections 3 and 4 of this paper, the layout process of optical fiber is determined as follows: grooving and burying the optical fiber in the primary lining (similar to the layout of optical fiber 5 in the test in this article); tying the optical fiber to the main reinforcement of the cage in the second lining (similar to the layout of optical fibers 1 and 4 in this test).

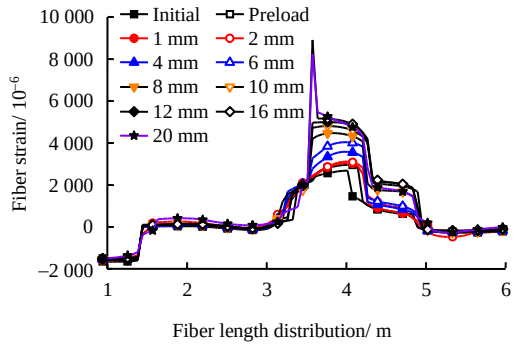

(a) Strain monitoring data of fiber 1

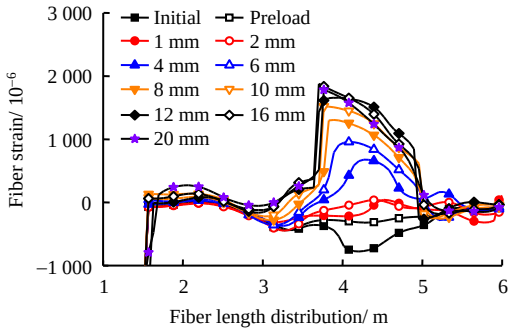

(b) Strain monitoring data of fiber 2

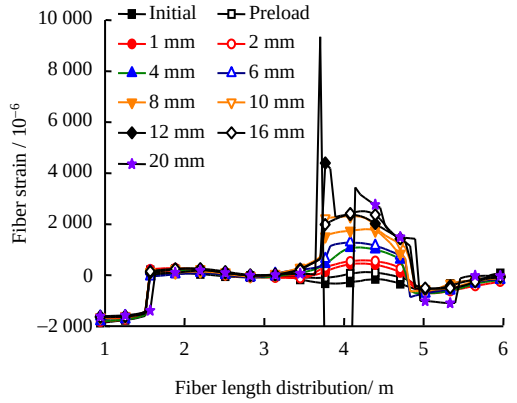

(c) Strain monitoring data of fiber 3

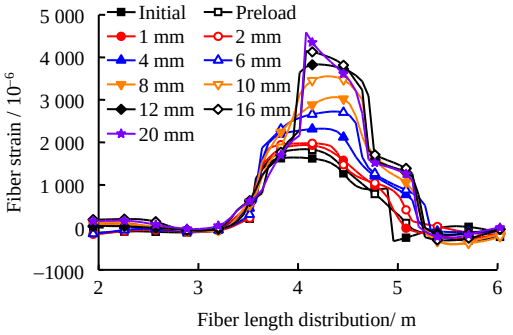

(d) Strain monitoring data of fiber 4

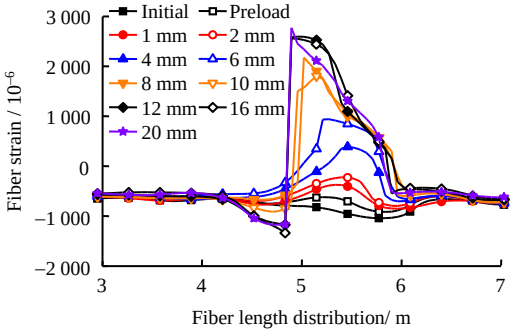

(e) Strain monitoring data of fiber 5

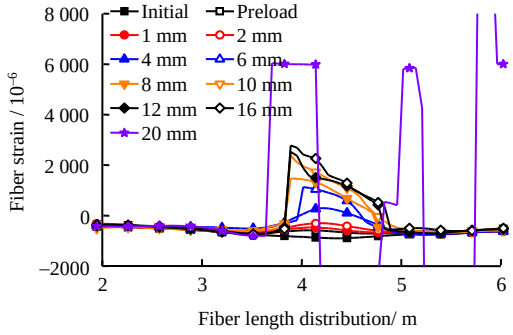

(f) Strain monitoring data of fiber 6

Fig.8 Fiber strain monitoring data of beam 1

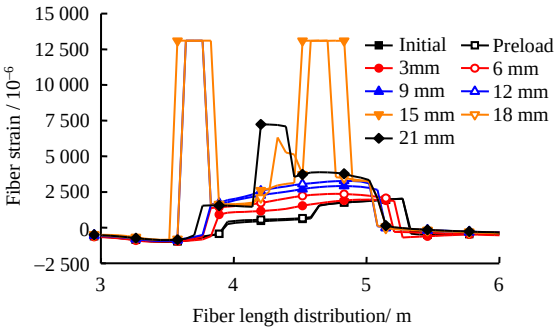

(a) Strain monitoring data of fiber 1

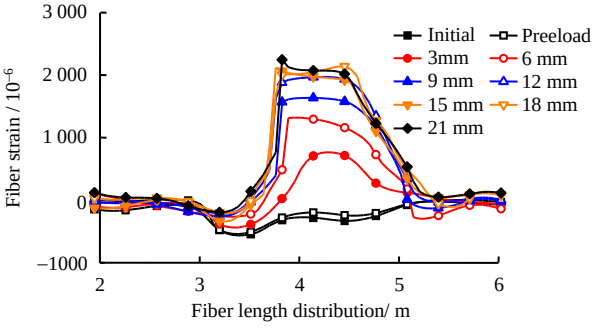

(b) Strain monitoring data of fiber 2

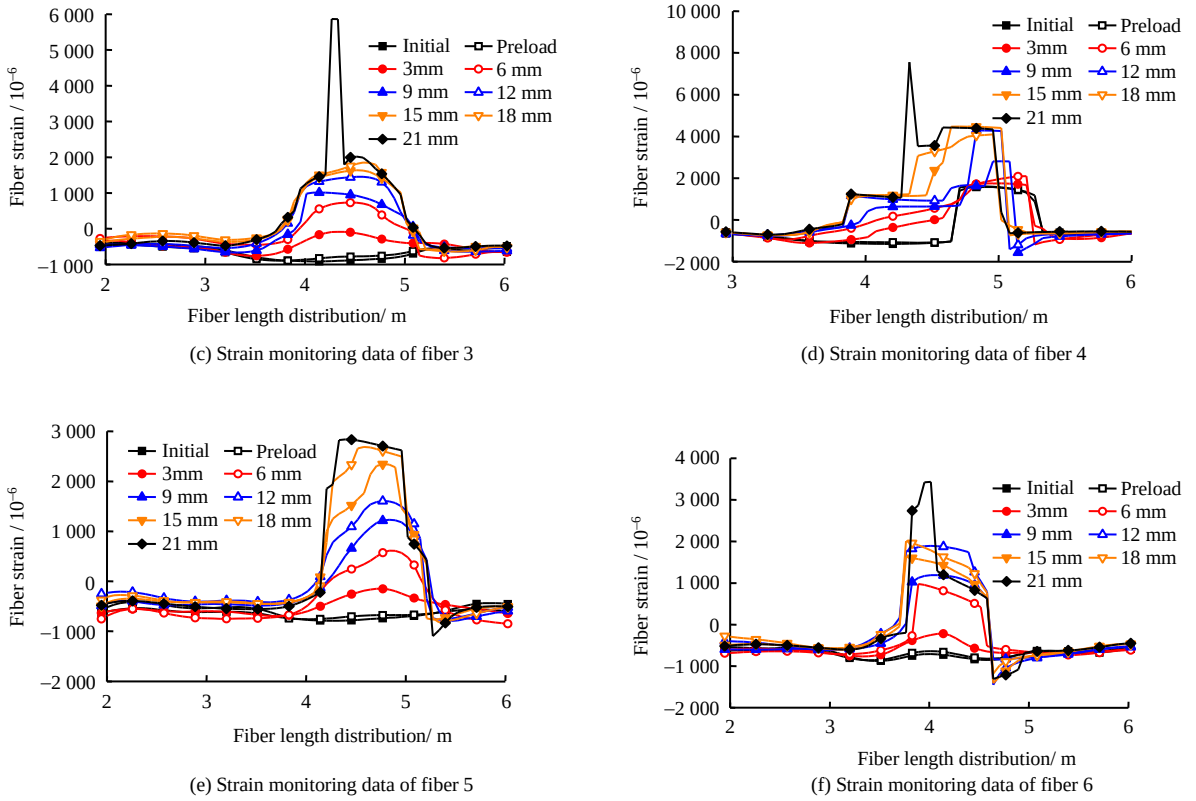

(c) Strain monitoring data of fiber 3

(d) Strain monitoring data of fiber 4

(e) Strain monitoring data of fiber 5

(f) Strain monitoring data of fiber 6

Fig.9 Fiber strain monitoring data of beam 2

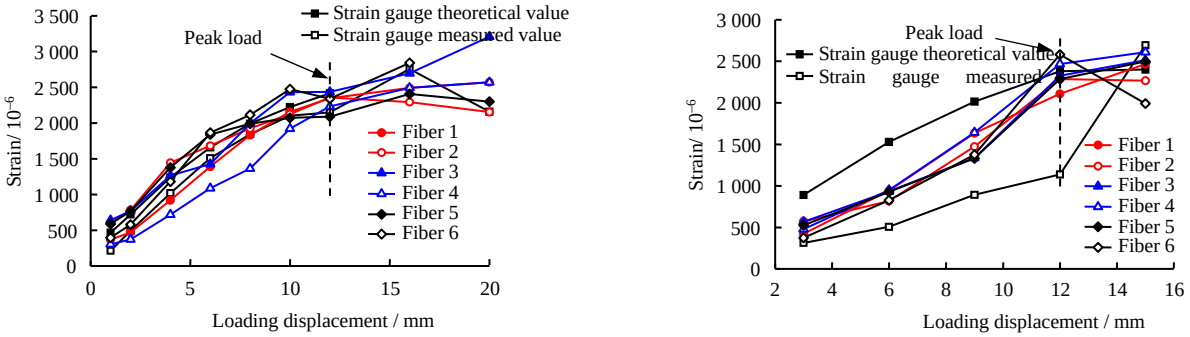

(a) Comparison of monitoring data of optical fiber and strain gauge in beam 1

(b) Comparison of monitoring data of optical fiber and strain gauge in beam 2

Fig.10 Comparison of monitoring data between optical fiber and strain gauge

The specific construction methods are as follows:

Primary lining: groove is made on the two waist and the vault of the primary lining, with the groove size (15 mm deep × 10 mm wide × full length of the concealed excavation section). After embedding the optical fiber, the quick setting high strength cement mortar is used for plugging. After 7 days of curing, non-destructive testing is carried out on the slotted sealing area and the original primary lining with a rebound tester. If the strength of the two is the same after testing, it can be considered that the slotted sealing area and the original primary lining structure have formed a whole. In order to eliminate the influence of temperature on the strain of optical fiber, temperature-compensated optical fiber is arranged along the tunnel length. The relevant construction process is shown in Fig. 11.

Second lining: the total length of the tunnel is about 91 m. Due to the use of alternative bay construction method, the second lining needs to be carried out in sections. Each segment of the second lining is 6 m long, with a total of 15 segments. There is a ring beam at the beginning and end of the tunnel. The optical fiber cannot be generally laid along the longitudinal direction of the tunnel, and only some relatively important segments (segments 1, 8 and 15) can be selected for laying. The first segment and the fifteenth segment are located at both ends of the concealed excavation section, and the eighth segment corresponds to a highway on the surface, so the first, the eighth

and the fifteenth segment are selected for laying optical fiber for deformation monitoring. In the secondary lining, the fiber is arranged along the direction (circumferential and longitudinal) of the main reinforcement in the upper semicircle reinforcement cage. The optical fiber is represented by a blue line in Fig. 12 (a). The actual construction is shown in Fig.12 (b).

6.3 Construction monitoring of removal of middle partition wall and middle floor

There is a risk of structural settlement in the process of breaking the middle partition wall and middle slab, so this process is selected for monitoring.

After the inverted arch concrete pouring is completed and the construction steps of the alternative bay construction method meet the construction conditions of the side wall and the vault, the temporary middle plate and the middle partition wall of the construction section will be broken. To reduce the construction wastes in the tunnel and shorten the suspension time of the primary lining vault, the scope of breaking the two sides of the middle plate is 1 m from the side wall of the primary lining to the tunnel, and the scope of breaking the mid-partition is 1.35 m below the vault. Figure 13 shows the scope of the removal of the middle partition and the comparison before and after the removal of the middle partition wall.

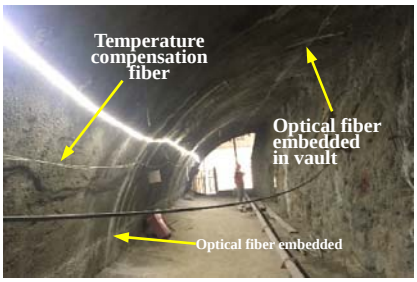

(a) Optical fibers embedded in waists and vault of primary lining

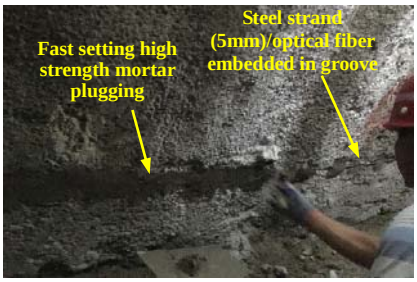

(b) Construction of optical fiber embedded in waists of primary lining

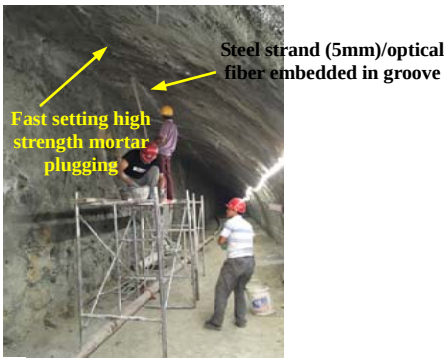

(c) Construction of optical fiber embedded in vault of primary lining

Fig.11 Optical fiber layout position and construction schematic in initial lining

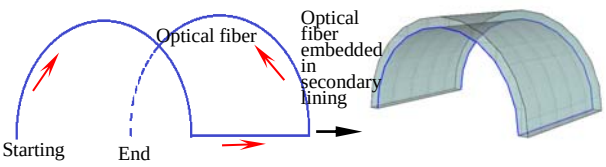

(a) Schematic diagram of optical fiber layout in secondary lining

(b) Construction drawing of optical fiber layout in secondary lining

Fig.12 Optical fiber layout position and construction drawing in second lining

6.4 Monitoring results and analysis of primary lining optical fiber

The construction of the second lining is divided into 15 segments. The monitoring results before and after the middle partition wall is removed at the first segment are shown in Fig.14.

Figure 14(a) shows the result of optical fiber monitoring on the vault. In segment 1, the strain value of optical fiber fluctuates in a range of 5 m long compared with that before the breaking of partition wall and middle plate. It can be precisely positioned. The calculated optical fiber deformation value is about 2.5 mm in the fluctuation range of 5 m, and the average strain value is about 500×10^{-6}. From Fig.14(a), it can be seen that after the middle partition wall and the middle plate are broken, the strain value of the optical fiber becomes smaller or even negative at the vault. After preliminary analysis, the reason can be attributed to the slight settlement of the vault due to the loss of part of the support of the middle partition wall, resulting in a small compression deformation of the optical fiber laid inside the initial lining. As the first section of the broken middle wall is located at the end of the tunnel, the optical fiber deformation is similar to that of the lower cantilever beam under pressure, with reference to Fig. 15. The calculated settlement of the initial lining is about 1.3 mm

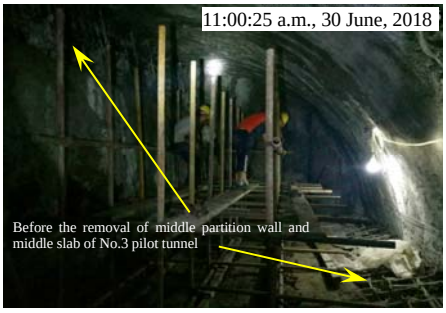

(a) Before the removal of middle partition wall and middle slab

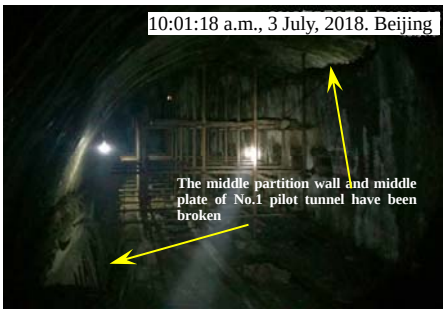

(b) After the removal of middle partition wall and middle slab

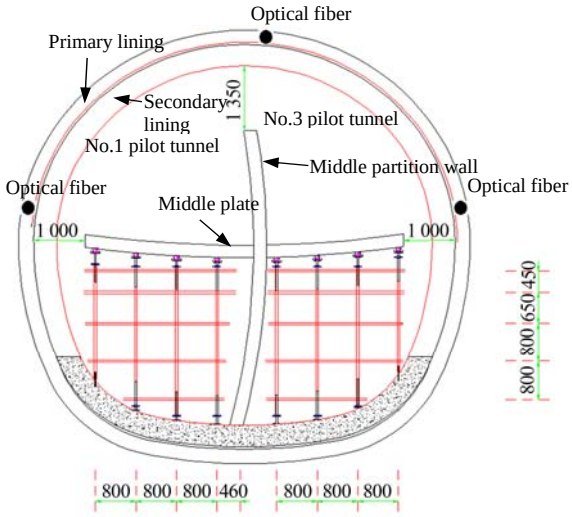

(c) Location of optical fiber layout and the scope of middle partition wall removal（unit：mm）

(d) On-site monitoring

Fig.13 Breaking and site monitoring of middle partition and middle plate

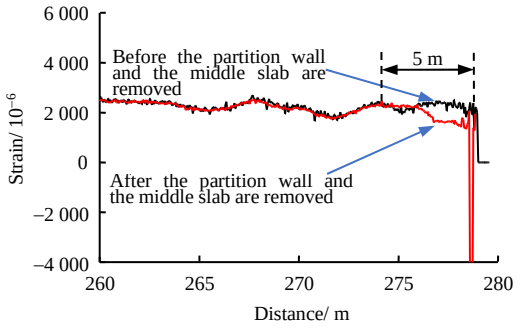

(a) Monitoring results of vault optical fibe

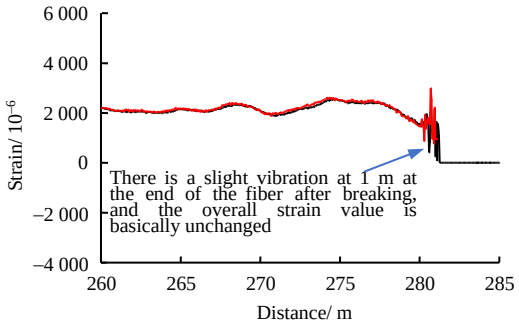

(b) Monitoring results of the optical fiber at the waist of No. 1 pilot tunnel

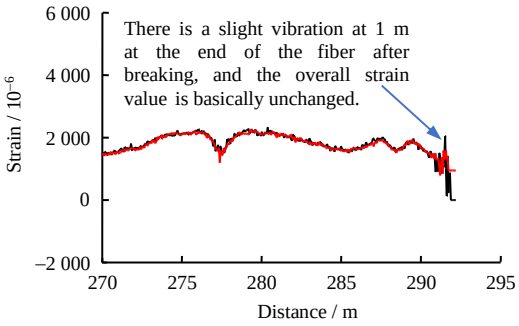

(c) Monitoring results of the optical fiber at the waist of No. 3 pilot tunnel

Fig.14 Results associated to the breakage of middle partition wall and mid-ply in optical fiber monitoring with primary lining

by using relevant geometric knowledge. In the construction site, the total station instrument and convergence meter are also used to regularly monitor the relevant deformation during construction. During the process of removing the partition wall in section 1, the total station instrument monitors the settlement at the vault with a value of about 1.0 mm, and there is no convergence and settlement deformation at both waists. Considering the existence of various errors, it can be considered that the results of optical fiber monitoring are consistent with those of total station monitoring.

Fig. 14 (b) and 14 (c) show the monitoring results of the optical fibers at the two waists of the initial lining. After the partition wall and the middle slab are broken, the strain value within 1 m of the fiber tail slightly oscillates, but the overall

strain value is basically unchanged. According to preliminary analysis, the removal of the partition wall and the middle slab has basically no effect on the deformation of the two waist parts of the initial lining.

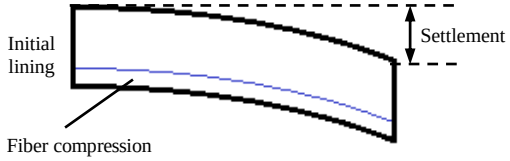

Fig.15 Optical fiber monitoring diagram of settlement deformation at the end of initial lining

6.5 Monitoring results and analysis of secondary lining optical fiber

Considering the objective factors such as construction and laying of optical fiber transmission line, the monitoring of optical fiber in the secondary lining needs to wait until the secondary lining is completed. After the completion of the second lining, the monitoring of the optical fiber in the second lining is carried out for a period of one month which is divided into 4 weeks. The monitoring is done once a week at a fixed time. The results are shown in Fig. 16.

Figure 16 shows the monitoring results of the optical fiber in the first, eighth and fifteenth segments of the second lining within one month after the completion of the second lining construction. There are six monitoring sections in the first, eighth and 15th segments of the second lining. It is found that the four monitoring data of any monitoring section fluctuate insignificantly (tens of micro-strains), which are basically consistent without obvious strain changes. It can be considered that no deformation has occurred, and the second lining structure has become stable.

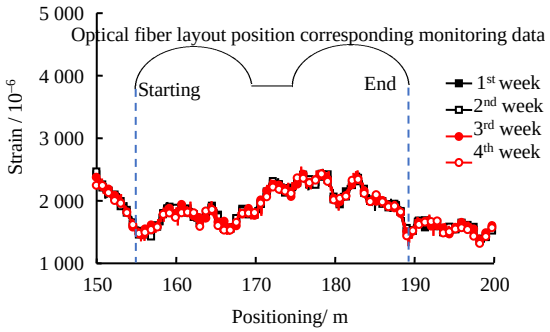

(a) Optical fiber monitoring data in the second lining of the first segment

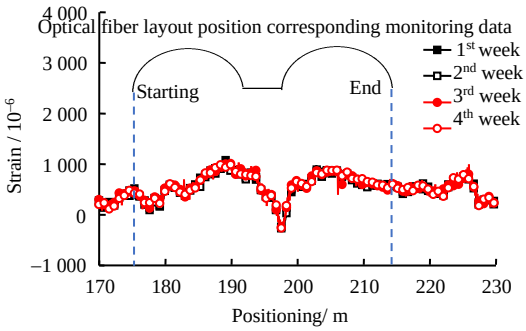

(b) Optical fiber monitoring data in the second lining of the eighth segment

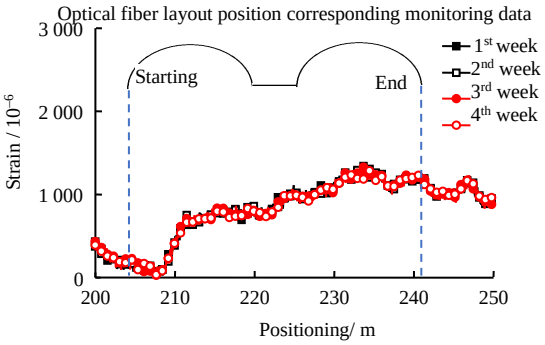

(c) Optical fiber monitoring data in the second lining of the fifteenth segment

Fig.16 Monitoring results of optical fibers in secondary lining

7 Conclusions

(1)Theoretical analysis shows that the strain transfer rate at both ends of the optical fiber is small, and that at the middle is the largest, which is close to 100%, and the overall shape is "convex". It is calculated that the strain transfer rate in the range of at least 90% of the length of the optical fiber can reach 95% when the embedded length of the optical fiber is greater than146 mm. A longer embedded length results in higher strain transfer efficiency. In distributed optical fiber monitoring engineering, the length of optical fiber is far more than 146 mm. Therefore, the difference caused by strain optical fiber types can be ignored. In theory, the overall strain transfer efficiency of embedded optical fiber can be considered to be close to 100%.

(2)The test results show that the layout of optical fiber has little effect on the monitoring results. The coupling between optical fiber and reinforced concrete beam is the best at the

stage before the steel bar begins to yield, and the coupling between optical fiber and beam is poor during the process of steel bar beginning to yield to the failure of the beam. The effective monitoring strain difference of embedded optical fiber is $3\ 000\times10^{-6}$, and that of optical fiber in other layouts is $2\ 000\times10^{-6}$. This strain difference is large enough to meet the requirements of most monitoring projects. In the actual monitoring project, the layout modes such as binding along the reinforcement cage and grooving -embedding in the concrete surface should be selected as far as possible.

(3)The application research on distributed strain optical fiber was performed in the subway tunnel of Beijing Rail Transit New Airport Line. A groove was formed on the inner surface of the primary lining, and the optical fiber was embedded into the slot and sealed with high-strength cement mortar. In the secondary lining, the optical fiber was tied along the main reinforcement of the reinforcement cage, and then concrete was poured. The monitoring results show that after removing the middle partition wall and middle slab in the first segment, the strain value of optical fiber at the initial lining vault changes significantly and the deformation position can be positioned accurately. The strain value of optical fiber at the two waists of the initial lining basically remains unchanged. The analysis shows that the settlement at the initial lining vault is caused by the construction of removing the middle partition wall and middle slab. The result of optical fiber monitoring in the secondary lining shows that the secondary lining basically does not deform after completion of construction and the overall structure tends to be stable.

(4)The application research shows that the layout methods of slotting-embedding optical fiber and binding optical fiber along the main reinforcement of the reinforcement cage in the secondary lining is feasible in the deformation monitoring project of the undercground tunnel.

References

[1] OHNO H, NARUSE H, KIHARA M, et al. Industrial applications of the BOTDR optical fiber strain sensor[J]. Optical Fiber Technology, 2001, 24(7): 45–64.

[2] SHI Bin, XU Xue-jun, WANG Di, et al. Study on BOTDR-based distributed optical fiber strain measurement for tunnel health diagnosis[J]. Chinese Journal of Rock Mechanics and Engineering, 2005, 24(15): 2622–2628.

[3] ZHANG Gui-sheng, MAO Jiang-hong, HE Yong, et al. Research on the tunnel deformation monitoring techniques based on BOTDA[J]. Highway, 2010, 54(2): 204–209.

[4] MA Shui-shan, WANG Zhi-wang, LI Duan-you, et al. Optical fiber sensors and their application to geotechnical engineering[J]. Chinese Journal of Rock Mechanics and Engineering, 2001, 20(Suppl.1): 1692–1694.

[5] CHAI Jing, ZHANG Ding-ding, LI Yi. Research progress of optical fiber sensing technology in geotechnical and geological engineering[J]. Journal of Architecture and Civil Engineering, 2015, 32(3): 28–37.

[6] LIU Yuan, LEI Tao, WANG Zhe, et al. Application of optical fiber sensing technology in mine safety monitoring[J]. Metal Mine, 2009, 38(Suppl.1): 536–538.

[7] LI Ming, WANG Xiao-lin, LÜ Gao-feng, et al. Development and application of optical fiber sensing technology in pipeline monitoring[J]. Contemporary Chemical Industry, 2014, 43(1): 54–57.

[8] YE Yu-xiao, YE Fang-jie, ZHAO Xin-ming, et al. Research on strain measuring in reinforced concrete beams with distributed optical fiber[J]. Low Temperature Architecture Technology, 2017, 39(3): 40–42.

[9] BAO Teng-fei, WANG Jia-lin, YAO Yuan. A fiber optic sensor for detecting and monitoring cracks in concrete structures[J]. Technological Sciences, 2010, 53(11): 3045–3050.

[10] HOU Gong-yu, XIE Bing-bing, HU Tao, et al. Fiber sheath effect in tunneling monitoring based on BOTDR technology[J]. Rock and Soil Mechanics, 2017, 38(8): 2441–2447.

[11] HOU Gong-yu, XIE Bing-bing, JIANG Yu-sheng, et al. Fiber sawtooth layout technology and principle used in roadway subsidence deformation monitoring[J]. Rock and Soil Mechanics, 2017, 38(Suppl.1): 96–102.

[12] LIU Yang. The research on monitoring technique of steel corrosion using fiber optic sensor[D]. Zhenjiang: Jiangsu University, 2009.

[13] CHEN Wen-hua, WANG Qun-min, ZHANG Yong-yong. Application of distributed optical fiber sensing to the lateral static load test on single pile[J]. Bulletin of science and technology, 2016, 32(8): 73–76.

[14] LI Rui, GAO Yuan, ZHOU Xi, et al. Application of distributed optical fiber sensing technology in internal force test of rotary digging bored pile body in Chengdu area[J]. Engineering Structure, 2017, 37(3): 163–166.

[15] LI Hong-nan, REN Liang. Fiber Bragg grating sensing technology for structural health monitoring[M]. Beijing: China Architecture & Building Press, 2008.

[16] ZHU Zhi-qun. The necessity of "tensile strain of longitudinal tensile steel bar to be 0.01" in flexural members[J]. Highways & Automotive Applications, 2016, 33(6): 88–90.